Atmospheric
Chemistry
and Physics
Discussions

Open Access

Size distribution and mixing state of black carbon particles during a heavy air pollution episode in Shanghai

X. Gong[1], C. Zhang[1], H. Chen[1], S. A. Nizkorodov[2], J. Chen[1,3], and X. Yang[1,3]

[1]Shanghai Key Laboratory of Atmospheric Particle Pollution and Prevention, Department of Environmental Science and Engineering, Fudan University, Shanghai 200433, China
[2]Department of Chemistry, University of California, Irvine, California 92697, USA
[3]Fudan-Tyndall Center, Fudan University, Shanghai 200433, China

Correspondence to: X. Yang (yangxin@fudan.edu.cn)

ACPD

15, 35383–35415, 2015

Size distribution and mixing state of BC particles in Shanghai

X. Gong et al.

Title Page

Abstract	Introduction
Conclusions	References
Tables	Figures

|◄ ►|

◄ ►

Back Close

Full Screen / Esc

Printer-friendly Version

Interactive Discussion

Full Screen / Esc

Printer-friendly Version

Interactive Discussion

Abstract

A Single Particle Aerosol Mass Spectrometer (SPAMS), a Single Particle Soot Photometer (SP2) and various meteorological instruments were employed to investigate the chemical and physical properties of black carbon (BC) aerosols during a regional air pollution episode in urban Shanghai over a five-day period in December 2013. The average $PM_{2.5}$ and BC mass concentrations were 221 and $3.2\,\mu g\,m^{-3}$, respectively, with the $PM_{2.5}$ peak value of $636\,\mu g\,m^{-3}$ at noon of 6 December and the BC peak value of $12.1\,\mu g\,m^{-3}$ at 04:26 LT on 7 December. The number size of BC cores was distributed over $\sim$ 60–400 nm, with a peak around $\sim$ 60 nm. The BC core mass size distribution was within $\sim$ 70–500 nm, with a peak around $\sim$ 200 nm.

The number concentration of BC-containing particles captured by SPAMS in the size range 200–1200 nm agreed very well with that detected by SP2 (R^2 = 0.87). A cluster analysis of the single particle mass spectra allowed for the separation of BC-containing particles into seven classes. Pure BC accounted for 0.53 % of BC-containing particles; BC attributed to biomass burning (BBBC) accounted for 22.60 %; K-rich BC-containing (KBC), NaK-rich BC-containing (NaKBC), BC internally-mixed with OC and ammonium sulfate (BCOC-SOx), BC internally-mixed with OC and ammonium nitrate (BCOC-NOx) were all attributed to traffic emissions and accounted for 73.24 %; unidentified particles accounted for 3.63 %.

The size distribution of internally-mixed BC particles was bimodal. Detected by SP2, the condensation mode peaked around $\sim$ 230 nm and droplet mode peaked around $\sim$ 380 nm, with a clear valley in the size distribution around $\sim$ 320 nm. The condensation mode mainly consisted of traffic emissions, with particles featuring a small BC core ($\sim$ 60–80 nm) and a relatively thin absolute coating thickness (ACT, $\sim$ 50–130 nm). The droplet mode included highly aged traffic emission particles and biomass burning particles. The highly aged traffic emissions had a small core ($\sim$ 60–80 nm) and a very thick ACT ($\sim$ 130–300 nm), which is larger than reported in any previous literature. The biomass burning particles had a larger BC core ($\sim$ 80–130 nm) and a thick ACT ($\sim$ 110–

300 nm). High concentration gaseous pollutants like NO_2 were found to accelerate the aging process and resulted in a continuous size growth of BC-containing particles from traffic emission. The condensation of gaseous pollutants made a significant contribution to the extremely high particulate matter during heavy pollution episode in the urban area.

1 Introduction

Aerosols represent the largest uncertainty in estimating radiative forcing of atmospheric species, through strongly affecting the energy balance of the Earth by scattering and/or absorbing solar radiation (Pöschl, 2005), and influencing cloud formation (Jacobson, 2006). Emitted from incomplete combustion of fossil fuel and biomass (Bond et al., 2013), black carbon (BC) is a strongly light-absorbing carbonaceous material in aerosols, second to carbon dioxide as a contributor to positive radiative forcing (Ramanathan and Carmichael, 2008; Jacobson, 2001).

The physical (e.g., size distribution and morphology) and chemical (e.g., mixing state and composition) properties of ambient BC are very complex and are constantly changing in the atmosphere. For example, BC particles exposed to sub-saturated sulfuric acid vapor exhibit a marked change in morphology, characterized by a decreased mobility-based diameter but an increased fractal dimension and effective density (Zhang et al., 2008). Through using electron tomography with a transmission electron microscope and three-dimensional (3-D) imaging, Adachi et al. (2010) found that many BC particles have open, chainlike morphology even after being surrounded by organic matter, and are located in off-center positions within their host materials. China et al. (2013) quantified the morphology of BC particles and classified them into four categories: ~ 50 % were embedded (heavily coated), ~ 34 % were partly coated, ~ 12 % had inclusions and ~ 4 % were bare. The organic coating is known to strongly affect the optical properties of the soot aggregates by acting as a lens that amplifies the absorption coefficient of the BC core (Lack and Cappa, 2010; Shiraiwa et al., 2010). Schnaiter

et al. (2005) observed that amplification factors of the internally-mixed BC of 1.8 to 2.1 compared to the specific absorption cross section of externally-mixed BC. Zhang et al. (2008) observed that the internally-mixed particles can increase their absorption efficiency by nearly 2-fold and scattering efficiency by approximately 10-fold at 80 % relative humidity relative to fresh particles. On the other hand, Cappa et al. (2012) and Lan et al. (2013) observed a limited enhancement due to the mixing state of ambient BC, suggesting that other factors may affect their absorption properties. Through coagulation and condensation, BC can form an internal mixture, which increases its cloud nucleation activity (Khalizov et al., 2009; Moffet and Prather, 2009). Most BC is removed from the troposphere via wet deposition with a short lifetime of 5 to 10 days (Kanakidou et al., 2005; Chung and Seinfeld, 2002).

Many measurement methods for BC particles have been developed and used in recent years (Petzold et al., 2013). Among them, the Single Particle Soot Photometer (SP2) has become increasingly recognized as a valuable tool for characterizing BC-containing particles (Stephens et al., 2003; Schwarz et al., 2006). SP2 can quantitatively measure the mass and determine the mixing state of an individual BC-containing particle (Schwarz et al., 2010). Taylor et al. (2014) quantitatively evaluated the capability of the SP2 to determine the particle mixing state through using the concentric core/shell model. Liu et al. (2014) analyzed the size distribution, mixing state of BC aerosols in London during winter time based on the same technique. Furthermore, Moteki et al. (2014) identified two morphological types of the mixed BC-containing particles as attached and coated, an important finding for understanding the climate impact of BC particles.

Depending on the experimental method, different terms are used in the literature for the most refractory and light-absorbing components of carbonaceous aerosols: black carbon (BC) or elemental carbon (EC). The definitions of EC and BC have been discussed in details elsewhere (Bond and Bergstrom, 2006; Almeida et al., 2013; Petzold et al., 2013). Herein, we use BC throughout this manuscript, since we applied SP2 to

Size distribution and mixing state of BC particles in Shanghai

X. Gong et al.

quantitatively measure the refractory black carbon mass, which utilizes laser-induced incandescence method (Petzold et al., 2013; Stephens et al., 2003).

As a highly complementary instrument, single particle mass spectrometer can detect the chemical properties of BC particles. Moffet and Prather (2009) observed a rapid coating process of organic carbon and sulfate on the BC core and assessed the related absorption enhancement during an air pollution episode of the Mexico City. Healy et al. (2012b) found that the mass size distribution for BC-containing particles was bimodal at an urban background site in Paris. The smaller mode was attributed to local emission, mostly externally-mixed BC particles, while the larger mode was dominated by aged particles associated with continental transport events. Zhang et al. (2014) found that an active photochemical formation of secondary organic aerosol (SOA) led to a distinct diurnal pattern of mixing state of BC with SOA in the condensation mode, while the photochemical aging had limited or negligible influence on the mixing state and growth of BC in the droplet mode. The size ranges of condensation mode ($D_{va} = \sim 100$–300 nm) and droplet mode ($D_{va} = \sim 300$–1000 nm) were defined by John et al. (1990) and Seinfeld and Pandis (2012).

Shanghai, with a population of over 24 million people, is the largest commercial and industrial mega-city in China. Due to the skyrocketing amount of industrial and metropolitan emissions, Shanghai's air quality has been deteriorating in the past decades. For example, the annual average $PM_{2.5}$ concentration was reported to increase from about $60\,\mu g\,m^{-3}$ during 1999–2000 to about $90\,\mu g\,m^{-3}$ in 2005–2006 (Ye et al., 2003; Feng et al., 2009). Previous aerosol studies in Shanghai were mostly based on filter sampling with a coarse time resolution, which cannot always keep track of the fast variation of aerosol properties in the atmosphere. In this study, we deployed two complementary techniques, with single particle resolution and high time resolution, to detect the evolution of the urban BC aerosols in Shanghai during an extreme pollution period. We used the SP2 to measure the mass and size distribution, and the mixing state of individual BC particles. Single Particle Aerosol Mass Spectrometer (SPAMS)

was used in parallel to record chemical characteristics and mixing state of individual BC particles.

2 Experimental

2.1 Single particle soot photometer

2.1.1 Description

The number and mass size distribution, as well as the mixing state of individual refractory BC particles were characterized using a single particle soot photometer (SP2, Droplet Measurement Technologies, Inc., Boulder, CO) (Stephens et al., 2003; Baumgardner et al., 2004). In brief, SP2 detects incandescence and scattering signals of BC-containing particles induced by a 1064 nm Nd:YAG intra-cavity laser. The mass of BC is proportional to the intensity of the laser induced incandescence signal. Any measured particle with a detectable incandescence signal is treated as a BC particle; whereas a particle that only exhibits scattering signal is considered as a non-BC particle. The total BC mass loading is reported as the sum of all detected single BC masses. The SP2 samples at low flow ($30 \, cm^3 \, min^{-1}$) in order to avoid multiple particles crossing the laser at the same time. We only saved data for every 50th particle in order to extend the sampling time without generating excessively large data sets.

2.1.2 Calibration and detection efficiency

The SP2 incandescence signal was calibrated using Aquadag[®] black carbon particles (Aqueous Deflocculated Acheson Graphite, manufactured by Acheson Inc., USA). The Aquadag[®] black carbon particles were selected by mobility diameter using a differential mobility analyzer (DMA) and the corresponding particle masses were calculated using the effective density data provided in Gysel et al. (2011). The scattering signal was calibrated using mono-disperse polystyrene latex spheres (Nanosphere Size Stan-

dards, Duke Scientific Corp., Palo Alto, CA, USA) with known diameters (80–350 nm). More details about SP2 calibration can be found in Gysel et al. (2011), Baumgardner et al. (2012) and Laborde et al. (2012). A diagram of the calibration system is shown in the Supplement (Fig. S1).

The detection efficiency was measured using Aquadag[®] black carbon particles, and the results were shown in Fig. S2 (in the Supplement). The details of the measurement method were described in Schwarz et al. (2010). SP2 detection efficiency was nearly unity for larger BC mass (up to 300 fg, corresponding to 680 nm mass-equivalent diameter). While the minimum BC mass with near-unity detection efficiency is ~ 0.7 fg BC-mass corresponding to 90 nm mass-equivalent diameter. The total ambient mass concentrations of BC were underestimated because of the low detection efficiency of the smaller BC particles, likely by $\sim 20\%$ (Schwarz et al., 2006; McMeeking et al., 2010). During the calibration and sampling time, the SP2 was operated at a stable temperature 20° and pressure ~ 1013 hPa. The SP2 laser power was at 1750 mA through the whole experiment.

2.1.3 Data analysis

The BC mass in individual particle was determined from the peak intensity of the incandescence signal according to the Aquadag[®] black carbon calibration (Sect. 2.1.2). The measured ambient BC mass was converted to the mass equivalent diameter, assuming a density of 1.8 g cm^{-3} (Bond and Bergstrom, 2006). In addition to the BC mass, the measurement of the scattering signal of a BC-containing particle allows for the determination of its scattering cross section. However, the scattering properties of externally- and internally-mixed BC particles, as detected by the SP2, may be distorted, because the mass of each particle is reduced by the laser heating. Thus, scattered light from a sampled BC particle does not yield a full Gaussian waveform. The Gaussian scattering function was reconstructed from the leading edge of the scattering signal (before the particle is perturbed by the laser) by using a two-element avalanche photodiode (APD). This method allows SP2 to determine the scattering properties of individual BC

particles as well as the BC mass and to distinguish the mixing state of a single BC particle (so called, LEO-fit method, Gao et al., 2007). The optical diameter of a BC particle or the coated BC size (D_p) was derived by inputting the LEO fitted scattering signal and BC core size (D_c) into Mie calculations, and using a core refractive index $m = 2.26–1.26i$ (Moteki et al., 2010; Liu et al., 2014; Laborde et al., 2013) and a coating refractive index $m = 1.5 + 0i$ (Laborde et al., 2013). The absolute coating thickness (ACT) of a BC particle was calculated as $(D_p – D_c)/2$. However, BC aging processes in the real atmosphere may result in aerosols with particles that have a off-centered morphology (Matsui et al., 2013). For example, when a small BC particle coagulates with a relatively large BC-free particle, the small BC particle may stay at the surface and lead to an effective negative coating thickness if determined by the methods used here. In this study, the negative coating thickness was observed for less than 2 % of all BC-containing particles; we did not take those particles into account when we calculated the average ACT. More details of data analysis and uncertainties are discussed in supplement, as well as in Liu et al. (2014) and Laborde et al. (2013).

2.2 Single particle aerosol mass spectrometer

A SPAMS was deployed simultaneously with SP2 to detect chemical composition of BC-containing particles. The technical details of SPAMS have been described elsewhere (Li et al., 2011). Briefly, aerosols in the size range of 0.2–2.0 µm are introduced into the focus lens through a 0.1 mm critical orifice at a flow of 80 mL min^{-1} due to the pressure drop from ~ 760 to ~ 2.2 Torr. Then particles are accelerated to a terminal size-dependent aerodynamic velocity, which is measured by two orthogonally-oriented continuous lasers (532 nm) separated by a fixed 6 cm distance. A pulsed desorption/ionization laser (Q-switched Nd:YAG laser, 266 nm) is triggered when a particle arrives at the ion source region. Both positive and negative ions are detected simultaneously by the time-of-flight mass spectrometer. In this work, the power of the desorption/ionization laser was kept at ~ 0.6 mJ per pulse. The particle size was calculated from the measured speed using a calibration curve generated by mono-disperse

polystyrene latex spheres (Nanosphere Size Standards, Duke Scientific Corp., Palo Alto, CA, USA) with known diameters (0.22–2.00 µm).

All single particle mass spectra were converted into a list of peaks at each m/z using TSI MS-Analyze software with a minimum signal threshold of 30 arbitrary units above the baseline. The resulting peak lists were then imported into YAADA (www.yaada.org), a software toolkit in Matlab (version R2012b) for further analysis of particle sizes and chemical components. A total of 385 683 particles were chemically analyzed with both positive and negative ion spectra, accounting for about 56 % of all sized particles. Based on the similarities of the mass-to-charge ratio and peak intensity, particles were clustered by using the ART-2a (adaptive resonance theory) method (Song et al., 1999) with a vigilance factor of 0.85, a learning rate of 0.05 and 20 iterations. Then BC-containing particles, with D_{va} in the size range of 0.2–1.2 mm, were chosen from the clusters, since this size range was consistent with the dominant fraction of BC-containing mass in the atmosphere (Zhang et al., 2014; Healy et al., 2012b). Then, total of 86 057 BC-containing particles were grouped into 7 general particle types according to mass spectral patterns.

2.3 Sampling period and site

The sampling lasted for almost 5 days, from 5 to 10 December 2013. The instruments were operated in the building of the Department of Environmental Science and Engineering, Fudan University (FDU, 31°14′ N, 121°29′ E) in urban Shanghai, close to both residential and traffic emissions sources. Aerosols were transferred to the instruments through a 6 m long stainless steel pipe (45 mm inner diameter) with the inlet positioned 2 m above the roof of the building. A cyclone pump was used to pull air through the sampling system at 30 L min^{-1}, minimizing particle residence time in the sampling line. Aerosols were dried by diffusion drying tubes before they reached the SP2 and SPAMS, which were connected in parallel. The measurement system is presented in Fig. S1 in the Supplement. Because of the extremely high particle mass loading, the inlets of SP2 and SPAMS were clogged two times during the sampling period.

3 Result and discussion

3.1 Overview of the meteorology

Temporal variations of measured relative humidity, temperature, CO, O_3, NO_2, SO_2, $PM_{2.5}$ and PM_{10} in Shanghai from 12:00 LT on 5 December to 14:00 LT on 10 December are shown in Fig. 1. The temperature and relative humidity varied between 2–19 °C and 30–100 % with an average of 10 °C and 73 %, respectively, during the study. The O_3 concentration was relatively low from 18:00 LT on 5 December to 08:00 LT on 7 December. The CO concentration showed two peaks during this period, and its peak value reached 4.1 µg m^{-3} at 14:00 LT on 6 December. The NO_2 concentration increased quickly at the beginning, reached 202.5 µg m^{-3} at 21:00 LT on 5 December, and then decreased slowly until 12:00 LT on 7 December. After 12:00 LT on 7 December, the concentrations of O_3, CO, NO_2 and SO_2 fluctuated irregularly. The concentrations of O_3 and NO_2 showed the expected anti-correlation, because NO was oxidized to NO_2 by O_3. The CO concentration was found to agree reasonably well with BC mass concentration ($R^2 = 0.59$, slope = 0.33), as shown in Fig. S3. Previous studies found that CO is a good marker of automobile emissions, which also produce BC (John et al., 1990; Long et al., 2003).

The mass loading of $PM_{2.5}$ was extremely high during this period. Its maximum value reached 636 µg m^{-3} at 12:00 LT on 6 December, which was a record-breaking hourly concentration for Shanghai. The daily average concentration was 221 µg m^{-3}. Meanwhile, PM_{10} varied from 47 to 691 µg m^{-3}, with an average of 252 µg m^{-3}. Concentrations of CO, O_3, NO_2, SO_2, PM_{10} and $PM_{2.5}$ during 5–10 December all exceeded the Chinese national ambient air quality standards.

3.2 BC size distributions and concentration measurement by SP2

We fitted a log-normal distribution for BC core number and mass size measurements, as shown in Fig. 2. The number size ranges from ~ 60 to ~ 400 nm and the peak is

around ∼ 60 nm. The measured number concentrations drops below 60 nm because the detection efficiency greatly decreases (Sect. 2.1.2) below this particle size. Using the same method, Schwarz et al. (2008) also found that the peak concentration is around 60 nm in boundary layer. The BC core mass size distribution has a peak around 200 nm, and the most BC mass is distributed between 70–500 nm.

As shown in Fig. 1, the BC mass concentration varied from 0.6 µg m^{-3} at 00:02 LT on 10 December to 12.1 µg m^{-3} at 04:26 LT on 7 December, with an average of 3.2 µg m^{-3}. The BC mass concentration observed in Shanghai is similar to other cities in China, e.g., ∼ 4.1 µg m^{-3} in Shenzhen (Huang et al., 2012) and ∼ 3.3 µg m^{-3} in Kaiping (Huang et al., 2011), however, it is much higher than in other mega-cities around the world, e.g., ∼ 0.9 µg m^{-3} in Paris (Laborde et al., 2013) and ∼ 1.3 µg m^{-3} in London (Liu et al., 2014). The BC mass accounted for 1.45 % of PM$_{2.5}$ mass on average in our measurements.

3.3 BC particles classification by SPAMS

Classification of particles analyzed by the SPAMS can help elucidate the sources, degree of aging, and mixing state of BC particles. We classified BC-containing particles into 7 groups according to their mass spectral characteristics. The names of these groups and their number fractions are shown in Table 1. The average mass spectral patterns of each group are showing in Fig. 3.

Pure BC particles only presented strong signals for black carbon fragment ions (C$_n^-$ and C$_n^+$) in both positive and negative ion mass spectra without any signal of secondary species like sulfate or nitrate, suggesting they were fresh BC particles that had not undergone any aging process.

Biomass burning BC-containing (BBBC) particles were characterized by an intense K$^+$ signal for +39 (the charge and m/z of the observed ion) in the positive ion mass spectra and a strong signal for –26 (CN$^-$) in the negative ion mass spectra. Typical black carbon fragments (C$_n^-$) appeared in the negative ion mass spectra. A high signal at –46 (NO$_2^-$), –62 (NO$_3^-$) and a relatively low signal at –97 (HSO$_4^-$) were also

observed, suggesting a significant accumulation of nitrite ions on BC particles through-out the air pollution period. Potassium-containing soot is a well-established tracer for biomass combustion (Andreae, 1983; Soto-Garcia et al., 2011). Particles with similar mass spectral patterns were previously observed in several urban field studies and as-signed to biomass burning sources (Moffet et al., 2008; Healy et al., 2012b; Bi et al., 2011).

BC internally-mixed with organic carbon and ammonium sulfate (BCOC-SOx) par-ticles exhibited signals for ammonium +17 (NH_3^+), +18 (NH_4^+), organic carbon +37 (C_3H^+), and a small signal for sodium +23 (Na^+) in the positive ion mass spectra, along with black carbon fragment ions (C_n^+). There was a high signal for sulfate −97 (HSO_4^-) and a relatively low signal for nitrate −46 (NO_3^-), −62 (NO_3^-) in the negative ion spectra. BC internally-mixed with organic carbon and ammonium nitrate (BCOC-NOx) particles are characterized by very similar positive ion mass spectra to BCOC-SOx, but exhibit lower signals for sulfate and higher signals for nitrate in the negative ion spectra, i.e., −46 (NO_3^-), −62 (NO_3^-). BC particles with various intensities for organic carbon, nitrate and sulfate were commonly detected in urban ATOFMS field studies (Moffet et al., 2008; Ault et al., 2009; Dall'Osto and Harrison, 2006) and were assigned to traffic emissions (Healy et al., 2012b).

K-rich BC-containing (KBC) particles exhibited strong signals for black carbon frac-tion in both positive and negative ion mass spectra. This class also had signals for potassium +39 (K^+) and ammonium +17 (NH_3^+), +18 (NH_4^+) in positive ion mass spec-tra and nitrate −46 (NO_2^-), −62 (NO_3^-), sulfate −97 (HSO_4^-) in the negative ion mass spectra. This class was detected from diesel vehicle emissions in previous study (Li et al., 2013).

NaK-rich BC-containing (NaKBC) particles exhibited signals for sodium +23 (Na^+), potassium +39 (K^+), and calcium +40 (Ca^+), along with black carbon fragment ions (C_n^-), sulfate −97 (HSO_4^-) and nitrate −46 (NO_2^-), −62 (NO_3^-) (Fig. 3). This class was de-tected in previous light/heavy-duty vehicle emission studies (Toner et al., 2006; Sode-man et al., 2005; Li et al., 2013).

We should note that SPAMS preferentially detected internally-mixed BC particles, and had reduced detection efficiency for pure BC particles. The particles detected and chemically analyzed by SPAMS range from 200 to 2000 nm in size, and the detection efficiency decreases rapidly below 400 nm and above 1200 nm (Li et al., 2011). The majority of the pure BC particles diameter are smaller than 200 nm in diameter (Kondo et al., 2006), and therefore, they are missed by SPAMS.

3.4 Mixing state and size distribution of internally-mixed BC particles

3.4.1 Temporal variations of internally-mixed BC particles

A comparison of the internally-mixed BC particles number concentration between SP2 and SPAMS is given in Fig. 4 and Fig. S4. The agreement observed is reasonably good ($R^2 = 0.87$, slope = 0.65) considering the combined experimental uncertainties of the methods. Detected by SP2, the internally-mixed BC particles accounted for approximately 70 % number fraction of BC-containing particles during the whole period. Moteki et al. (2007) also found the internally-mixed BC particles accounted for 63 % number fraction of BC-containing particles in the aged urban plume. The high correlation coefficient indicates that we can use the two complementary techniques to analyze the mixing state and chemical composition of internally-mixed BC particles with single particle resolution at the same time (although not for the same particle since both methods are destructive).

The temporal variation of number size distribution and particle types changed rapidly and intricately, as shown in Fig. 4. From 12:00 LT on 5 December to 00:00 LT on 7 December, the PM$_{2.5}$ and BC mass increased slowly to an extremely polluted state. The number fraction of BBBC particles also increased during this period (Fig. 4b) and the D_p of BC showed two distinct modes (Fig. 4a). Then, the BC-containing particles number increased rapidly at 02:00 LT on 7 December. Presumably, boundary layer compression during the night led the fast change of BC-containing particles. After that, the

number concentration of BC-containing particles exhibited diurnal variation, with two major peaks at the rush hours, i.e., from 08:00–12:00 LT or from 16:00–20:00 LT.

3.4.2 Size distribution and source apportionments of internally-mixed BC particles

Figure 5a shows the D_p number size distribution histogram detected by SP2. The BC-containing particles were detected in both the condensation and droplet modes in this study. The condensation mode peak was centered around ~ 230 nm and droplet mode peak was centered around ~ 380 nm, with a boundary D_p around ~ 320 nm. The presence of condensation mode ($D_{va} = \sim 200$–500 nm) and droplet mode ($D_{va} = \sim 550$–1200 nm) was confirmed by the SPAMS data (Fig. 5b). Similar particle size distributions were also found in other studies in China (Huang and Yu, 2008; Zhang et al., 2014).

The specific composition in condensation and droplet modes were quite different (Fig. 5b). BBBC particles exhibited a smaller number fraction in the condensation mode and dominated the number fraction in the droplet mode. Ammonium nitrate can condense on particle surfaces during atmospheric transport if sulfate is fully neutralized and excess ammonia is available (Riemer et al., 2004). The sulfate condensation on BC surfaces occurs rapidly at a local level, while ammonium nitrate condensation occurs continuously over longer timescales during transport (Healy et al., 2012a). Therefore, BCOC-NOx particles are much older than BCOC-SOx, and consequently have a larger size. As shown in Fig. 5b, the BCOC-NOx had a higher number fraction than BCOC-SOx did in the droplet mode. Based on the particle classification and source apportionment analysis, the internally-mixed BC particles from traffic emissions accounted for almost all of the particles observed in the condensation mode. However, the particle sources in the droplet mode were more diverse, including traffic emissions and biomass burning.

Previous studies revealed that different sources emit different core diameters for BC-containing particles (Liu et al., 2014; Takahama et al., 2014; Reddington et al., 2013; Schwarz et al., 2008) and the aging processes affect the coating thickness (Laborde

et al., 2013; Liu et al., 2014). We identified the sources and estimated aging process of BC-containing particles by using 2-D image plot "fingerprint" of D_c and absolute coating thickness (ACT) information. Figure 5c shows the dependence of ACT on D_c, weighed by the number concentration. In the condensation mode, the particles were character-ized by small D_c values (~ 60–80 nm) with thin ACT (~ 50–130 nm). In combination with the SPAMS information, these particles with small D_c with thin ACT should be mainly from the traffic sources (Fig. 5b).

However, the droplet mode was very different from the condensation mode and showed a diversity of sources. In the droplet mode, the "fingerprint" showed two peaks. The first peak had small D_c values (~ 60–80 nm) and thick ACT (~ 130–300 nm). We assume that the BC-containing particles in the first peak were from traffic emissions. In previous studies, the particles associated with traffic emissions had small core sizes and thin coating thickness (Laborde et al., 2013; Liu et al., 2014). However, in this study, we found that the BC-containing particles from traffic could be highly-aged, resulting in a much thicker coating than previously observed. This could be because polluted air masses promote faster BC aging processes (Matsui et al., 2013). The second peak showed larger D_c (~ 80–130 nm) and thick ACT (~ 110–300 nm). These particles were presumably from biomass burning. It has been reported using SP2 measurements that fresh biomass burning BC particles are thickly coated (Schwarz et al., 2008; Sahu et al., 2012; Liu et al., 2014).

Since there was no clear-cut separation between traffic emissions and biomass burn-ing BC-containing particle in droplet mode, it was hard to distinguish them when we just used the core and shell information from SP2 (Liu et al., 2014). We selected those larger core (80–130 nm) with thicker coating (120–300 nm) particles as biomass burn-ing particles and compared with the biomass burning particles number concentration from SPAMS, as shown in Fig. S5. The good agreement ($R^2 = 0.71$) verified the con-clusion that the BC-containing particles with bigger core and thicker coating were from biomass burning. Even though these larger BC-containing particles only accounted for less than 20 % number fraction, they are more likely to exhibit larger hygroscopicity

Title Page

Abstract | Introduction

Conclusions | References

Tables | Figures

|◄ | ►|

◄ | ►

Back | Close

Full Screen / Esc

Printer-friendly Version

Interactive Discussion

(Liu et al., 2013; Wang et al., 2014) and to be scavenged by wet deposition (Moteki et al., 2012). Besides, those particles will also have greater potential to enhance the semi-direct effect (Koch and Del Genio, 2010) through interaction with cloud processes.

The diversity of sources of the droplet mode BC-containing particles was also detected in SPAMS, as we discussed before. SPAMS data showed that, in the droplet mode, the internally-mixed BC particles from traffic emissions were more abundant than those form biomass burning (Fig. 5b). However, the SP2 data showed that particles with a small core and thick ACT (major traffic emission) were less abundant than particles with a larger core with thick ACT (major biomass burning) (Fig. 5c). As we discussed in part 2.1.2, BC-containing particle with smaller cores are not efficiently detected by SP2, which may result in an underestimation of the fraction of traffic emission BC-containing particles in the droplet mode.

The aging of traffic-emitted BC-containing particles during the heavy air pollution episode (12:00, 5 December 2013–12:00, 7 December 2013) was elucidated using the temporal variation of relative coating thickness (RCT, entire particle diameter/BC core diameter, D_p/D_c) of BC-containing particles ($D_c = 60$–80 nm), as shown in Fig. 6a. From 16:00 LT to 22:00 LT on 5 December, the RCT of BC-containing particles and PM$_{2.5}$ concentration grew rapidly. Even though the SP2's inlet was blocked from 23:00 LT on 5 December to 10:00 LT on 6 December due to the extremely high PM mass loading, the data collected around that time suggest the BC-containing particles growth was continuous until 13:00 LT on 6 December. The absolute coating growth rate was around 20 nm h^{-1} during this period (16:00, 5 December 2013–13:00, 6 December 2013). Variations of the major chemical species in the vehicle-emitted BC-containing particles (selected by SPAMS) were also analyzed. The relative peak areas of nitrate -63 (NO$_3^-$) and organic carbon (i.e., $+27$ (C$_2$H$_3^+$), $+43$ (CH$_3$CO$^+$)) showed significant incensement during this period (Fig. 6b). Guo et al. (2014) had observed that gaseous emissions of volatile organic compounds, nitrogen oxides from urban transportation and sulfur dioxide from region industry were responsible for large secondary particle matter formation in Beijing. In this work, the evaluation of BC-containing parti-

cles also suggested that high concentrations of gaseous pollutants like NO_2 or volatile organics and their transformations play a vital role for particle growth and the increase of PM loading in urban area especially during a heavy pollution episode. Reductions in the emissions of gaseous precursors, such as NO_2 in the urban area, are critical for
5   remediation of the severe urban haze pollution in China.

4   Conclusions

In this study, we characterized BC-containing particles during a heavy air pollution episode in Shanghai. The BC mass loading in Shanghai was similar to other cities in China but much higher than in other mega-cities around the world, with an average of
10   $3.2\,\mu g\,m^{-3}$ and the peak value of $12.1\,\mu g\,m^{-3}$ at 04:26 LT on 7 December 2013. The BC mass accounted for 1.45 % of $PM_{2.5}$ mass on average. The number- and mass-weighted BC core size distributions were around ~ 60–400 and 70–500 nm, with peaks around ~ 60 and ~ 200 nm, respectively.

    Through SPAMS, we classified the BC-containing particles into 7 groups, accord-
15   ing to their mass spectral patterns. The pure BC particles accounted for 0.53 % number fraction of BC-containing particles (although this number could be underestimated because of the low detection efficiency for pure BC in SPAMS). The BBBC particles came from biomass burning, accounting for 22.60 %. The KBC, NaKBC, BCOC-NOx and BCOC-SOx came from traffic emissions, accounting for 73.24 %. The remaining
20   unidentified particles accounted for 3.63 %.

    The size distribution of internally-mixed BC particles was bimodal. The condensation mode mainly consisted of traffic emissions, which had a small core (~ 60–80 nm) with thin ACT (~ 50–130 nm). The droplet mode included biomass burning and deeply aged traffic-emitted BC-containing particles. The biomass burning particles had larger
25   core sizes (~ 80–130 nm) with thick ACT (~ 110–300 nm) and the highly aged traffic emissions had small core sizes (~ 60–80 nm) with thick ACT (~ 130–300 nm). It is rare to see the traffic-emitted BC growing so quickly to the droplet mode. The high concen-

trations of gaseous pollutants like NO_2 and volatile organics and their transformations accelerated the growth of BC-containing particles and contributed to the high particle mass concentration in the heavy air pollution episode.

The quantitative number and mass information provided by SP2 supplemented the SPAMS chemical analysis in the entire experiment. The two complementary techniques can detect the physical and chemical properties of BC aerosol with single particle resolution. The combined use of SP2 and SPAMS would have potential of wider applications for future projects.

The Supplement related to this article is available online at doi:10.5194/acpd-15-35383-2015-supplement.

References

Adachi, K., Chung, S. H., and Buseck, P. R.: Shapes of soot aerosol particles and implications for their effects on climate, J. Geophys. Res.-Atmos., 115, D15206, doi:10.1029/2009JD012868, 2010.

Almeida, J., Schobesberger, S., Kurten, A., Ortega, I. K., Kupiainen-Maatta, O., Praplan, A. P., Adamov, A., Amorim, A., Bianchi, F., Breitenlechner, M., David, A., Dommen, J., Donahue, N. M., Downard, A., Dunne, E., Duplissy, J., Ehrhart, S., Flagan, R. C., Franchin, A., Guida, R., Hakala, J., Hansel, A., Heinritzi, M., Henschel, H., Jokinen, T., Junninen, H., Kajos, M., Kangasluoma, J., Keskinen, H., Kupc, A., Kurten, T., Kvashin, A. N., Laaksonen, A., Lehtipalo, K., Leiminger, M., Leppa, J., Loukonen, V., Makhmutov, V., Mathot, S., McGrath, M. J., Nieminen, T., Olenius, T., Onnela, A., Petaja, T., Riccobono, F., Riipinen, I., Rissanen, M., Rondo, L., Ruuskanen, T., Santos, F. D., Sarnela, N., Schallhart, S.,

Schnitzhofer, R., Seinfeld, J. H., Simon, M., Sipila, M., Stozhkov, Y., Stratmann, F., Tome, A., Trostl, J., Tsagkogeorgas, G., Vaattovaara, P., Viisanen, Y., Virtanen, A., Vrtala, A., Wagner, P. E., Weingartner, E., Wex, H., Williamson, C., Wimmer, D., Ye, P. L., Yli-Juuti, T., Carslaw, K. S., Kulmala, M., Curtius, J., Baltensperger, U., Worsnop, D. R., Vehkamaki, H., and Kirkby, J.: Molecular understanding of sulphuric acid-amine particle nucleation in the atmosphere, Nature, 502, 359–363, doi:10.1038/nature12663, 2013.

Andreae, M. O.: Soot carbon and excess fine potassium: long-range transport of combustion-derived aerosols, Science, 220, 1148–1151, doi:10.1126/science.220.4602.1148, 1983.

Ault, A. P., Moore, M. J., Furutani, H., and Prather, K. A.: Impact of emissions from the Los Angeles port region on San Diego air quality during regional transport events, Environ. Sci. Technol., 43, 3500–3506, doi:10.1021/es8018918, 2009.

Baumgardner, D., Kok, G., and Raga, G.: Warming of the Arctic lower stratosphere by light absorbing particles, Geophys. Res. Lett., 31, L06117, doi:10.1029/2003gl018883, 2004.

Baumgardner, D., Popovicheva, O., Allan, J., Bernardoni, V., Cao, J., Cavalli, F., Cozic, J., Diapouli, E., Eleftheriadis, K., Genberg, P. J., Gonzalez, C., Gysel, M., John, A., Kirchstetter, T. W., Kuhlbusch, T. A. J., Laborde, M., Lack, D., Müller, T., Niessner, R., Petzold, A., Piazzalunga, A., Putaud, J. P., Schwarz, J., Sheridan, P., Subramanian, R., Swietlicki, E., Valli, G., Vecchi, R., and Viana, M.: Soot reference materials for instrument calibration and intercomparisons: a workshop summary with recommendations, Atmos. Meas. Tech., 5, 1869–1887, doi:10.5194/amt-5-1869-2012, 2012.

Bi, X. H., Zhang, G. H., Li, L., Wang, X. M., Li, M., Sheng, G. Y., Fu, J. M., and Zhou, Z.: Mixing state of biomass burning particles by single particle aerosol mass spectrometer in the urban area of PRD, China, Atmos. Environ., 45, 3447–3453, doi:10.1016/j.atmosenv.2011.03.034, 2011.

Bond, T. C. and Bergstrom, R. W.: Light absorption by carbonaceous particles: An investigative review, Aerosol Sci. Tech., 40, 27–67, doi:10.1080/02786820500421521, 2006.

Bond, T. C., Doherty, S. J., Fahey, D. W., Forster, P. M., Berntsen, T., DeAngelo, B. J., Flanner, M. G., Ghan, S., Karcher, B., Koch, D., Kinne, S., Kondo, Y., Quinn, P. K., Sarofim, M. C., Schultz, M. G., Schulz, M., Venkataraman, C., Zhang, H., Zhang, S., Bellouin, N., Guttikunda, S. K., Hopke, P. K., Jacobson, M. Z., Kaiser, J. W., Klimont, Z., Lohmann, U., Schwarz, J. P., Shindell, D., Storelvmo, T., Warren, S. G., and Zender, C. S.: Bounding the role of black carbon in the climate system: A scientific assessment, J. Geophys. Res.-Atmos., 118, 5380–5552, doi:10.1002/jgrd.50171, 2013.

Title Page

Abstract | Introduction

Conclusions | References

Tables | Figures

Back | Close

Full Screen / Esc

Printer-friendly Version

Interactive Discussion

Cappa, C. D., Onasch, T. B., Massoli, P., Worsnop, D. R., Bates, T. S., Cross, E. S., Davidovits, P., Hakala, J., Hayden, K. L., Jobson, B. T., Kolesar, K. R., Lack, D. A., Lerner, B. M., Li, S. M., Mellon, D., Nuaaman, I., Olfert, J. S., Petaja, T., Quinn, P. K., Song, C., Subramanian, R., Williams, E. J., and Zaveri, R. A.: Radiative Absorption Enhancements Due to the Mixing State of Atmospheric Black Carbon, Science, 337, 1078–1081, doi:10.1126/science.1223447, 2012.

China, S., Mazzoleni, C., Gorkowski, K., Aiken, A. C., and Dubey, M. K.: Morphology and mixing state of individual freshly emitted wildfire carbonaceous particles, Nature Communications, 4, 2122, doi:10.1038/ncomms3122, 2013.

Chung, S. H. and Seinfeld, J. H.: Global distribution and climate forcing of carbonaceous aerosols, J. Geophys. Res.-Atmos., 107, 4407, doi:10.1029/2001JD001397, 2002.

Dall'Osto, M. and Harrison, R. M.: Chemical characterisation of single airborne particles in Athens (Greece) by ATOFMS, Atmos. Environ., 40, 7614–7631, doi:10.1016/j.atmosenv.2006.06.053, 2006.

Feng, Y., Chen, Y., Guo, H., Zhi, G., Xiong, S., Li, J., Sheng, G., and Fu, J.: Characteristics of organic and elemental carbon in $PM_{2.5}$ samples in Shanghai, China, Atmos. Res., 92, 434–442, doi:10.1016/j.atmosres.2009.01.003, 2009.

Gao, R., Schwarz, J., Kelly, K., Fahey, D., Watts, L., Thompson, T., Spackman, J., Slowik, J., Cross, E., and Han, J.-H.: A novel method for estimating light-scattering properties of soot aerosols using a modified single-particle soot photometer, Aerosol Sci. Tech., 41, 125–135, 2007.

Guo, S., Hu, M., Zamora, M. L., Peng, J., Shang, D., Zheng, J., Du, Z., Wu, Z., Shao, M., Zeng, L., Molina, M. J., and Zhang, R.: Elucidating severe urban haze formation in China, P. Natl. Acad. Sci. USA, 111, 17373–17378, doi:10.1073/pnas.1419604111, 2014.

Gysel, M., Laborde, M., Olfert, J. S., Subramanian, R., and Gröhn, A. J.: Effective density of Aquadag and fullerene soot black carbon reference materials used for SP2 calibration, Atmos. Meas. Tech., 4, 2851–2858, doi:10.5194/amt-4-2851-2011, 2011.

Healy, R. M., Chen, Y., Kourtchev, I., Kalberer, M., O'Shea, D., and Wenger, J. C.: Rapid formation of secondary organic aerosol from the photolysis of 1-nitronaphthalene: role of naphthoxy radical self-reaction, Environ. Sci. Technol., 46, 11813–11820, doi:10.1021/es302841j, 2012a.

Healy, R. M., Sciare, J., Poulain, L., Kamili, K., Merkel, M., Müller, T., Wiedensohler, A., Eckhardt, S., Stohl, A., Sarda-Estève, R., McGillicuddy, E., O'Connor, I. P., Sodeau, J. R., and

Size distribution and mixing state of BC particles in Shanghai

X. Gong et al.

Title Page

Abstract | Introduction

Conclusions | References

Tables | Figures

Back | Close

Full Screen / Esc

Printer-friendly Version

Interactive Discussion

Wenger, J. C.: Sources and mixing state of size-resolved elemental carbon particles in a European megacity: Paris, Atmos. Chem. Phys., 12, 1681–1700, doi:10.5194/acp-12-1681-2012, 2012.

Huang, X.-F. and Yu, J. Z.: Size distributions of elemental carbon in the atmosphere of a coastal urban area in South China: characteristics, evolution processes, and implications for the mixing state, Atmos. Chem. Phys., 8, 5843–5853, doi:10.5194/acp-8-5843-2008, 2008.

Huang, X. F., Gao, R. S., Schwarz, J. P., He, L. Y., Fahey, D. W., Watts, L. A., McComiskey, A., Cooper, O. R., Sun, T. L., Zeng, L. W., Hu, M., and Zhang, Y. H.: Black carbon measurements in the Pearl River Delta region of China, J. Geophys. Res.-Atmos., 116, D12208, doi:10.1029/2010jd014933, 2011.

Huang, X. F., Sun, T. L., Zeng, L. W., Yu, G. H., and Luan, S. J.: Black carbon aerosol characterization in a coastal city in South China using a single particle soot photometer, Atmos. Environ., 51, 21–28, doi:10.1016/j.atmosenv.2012.01.056, 2012.

Jacobson, M. Z.: Strong radiative heating due to the mixing state of black carbon in atmospheric aerosols, Nature, 409, 695–697, 2001.

Jacobson, M. Z.: Effects of externally-through-internally-mixed soot inclusions within clouds and precipitation on global climate, J. Phys. Chem.-USA, 110, 6860–6873, doi:10.1021/jp056391r, 2006.

John, W., Wall, S. M., Ondo, J. L., and Winklmayr, W.: Modes in the size distributions of atmospheric inorganic aerosol, Atmos. Environ. A-Gen., 24, 2349–2359, doi:10.1016/0960-1686(90)90327-j, 1990.

Kanakidou, M., Seinfeld, J. H., Pandis, S. N., Barnes, I., Dentener, F. J., Facchini, M. C., Van Dingenen, R., Ervens, B., Nenes, A., Nielsen, C. J., Swietlicki, E., Putaud, J. P., Balkanski, Y., Fuzzi, S., Horth, J., Moortgat, G. K., Winterhalter, R., Myhre, C. E. L., Tsigaridis, K., Vignati, E., Stephanou, E. G., and Wilson, J.: Organic aerosol and global climate modelling: a review, Atmos. Chem. Phys., 5, 1053–1123, doi:10.5194/acp-5-1053-2005, 2005.

Khalizov, A. F., Zhang, R., Zhang, D., Xue, H., Pagels, J., and McMurry, P. H.: Formation of highly hygroscopic soot aerosols upon internal mixing with sulfuric acid vapor, J. Geophys. Res.-Atmos., 114, D05208, doi:10.1029/2008JD010595, 2009.

Koch, D. and Del Genio, A. D.: Black carbon semi-direct effects on cloud cover: review and synthesis, Atmos. Chem. Phys., 10, 7685–7696, doi:10.5194/acp-10-7685-2010, 2010.

Kondo, Y., Komazaki, Y., Miyazaki, Y., Moteki, N., Takegawa, N., Kodama, D., Deguchi, S., Nogami, M., Fukuda, M., Miyakawa, T., Morino, Y., Koike, M., Sakurai, H., and Ehara, K.:

Temporal variations of elemental carbon in Tokyo, J. Geophys. Res.-Atmos., 111, D12205, doi:10.1029/2005JD006257, 2006.

Laborde, M., Schnaiter, M., Linke, C., Saathoff, H., Naumann, K.-H., Möhler, O., Berlenz, S., Wagner, U., Taylor, J. W., Liu, D., Flynn, M., Allan, J. D., Coe, H., Heimerl, K., Dahlkötter, F., Weinzierl, B., Wollny, A. G., Zanatta, M., Cozic, J., Laj, P., Hitzenberger, R., Schwarz, J. P., and Gysel, M.: Single Particle Soot Photometer intercomparison at the AIDA chamber, Atmos. Meas. Tech., 5, 3077–3097, doi:10.5194/amt-5-3077-2012, 2012.

Laborde, M., Crippa, M., Tritscher, T., Jurányi, Z., Decarlo, P. F., Temime-Roussel, B., Marchand, N., Eckhardt, S., Stohl, A., Baltensperger, U., Prévôt, A. S. H., Weingartner, E., and Gysel, M.: Black carbon physical properties and mixing state in the European megacity Paris, Atmos. Chem. Phys., 13, 5831–5856, doi:10.5194/acp-13-5831-2013, 2013.

Lack, D. A. and Cappa, C. D.: Impact of brown and clear carbon on light absorption enhancement, single scatter albedo and absorption wavelength dependence of black carbon, Atmos. Chem. Phys., 10, 4207–4220, doi:10.5194/acp-10-4207-2010, 2010.

Lan, Z. J., Huang, X. F., Yu, K. Y., Sun, T. L., Zeng, L. W., and Hu, M.: Light absorption of black carbon aerosol and its enhancement by mixing state in an urban atmosphere in South China, Atmos. Environ., 69, 118–123, doi:10.1016/j.atmosenv.2012.12.009, 2013.

Li, L., Huang, Z., Dong, J., Li, M., Gao, W., Nian, H., Fu, Z., Zhang, G., Bi, X., Cheng, P., and Zhou, Z.: Real time bipolar time-of-flight mass spectrometer for analyzing single aerosol particles, Int. J. Mass Spectrom., 303, 118–124, doi:10.1016/j.ijms.2011.01.017, 2011.

Li, L., Tan, G. B., Zhang, L., Fu, Z., Nian, H. Q., Huang, Z. X., Zhou, Z., and Li, M.: Analysis of diesel exhaust particles using single particle aerosol mass spectrometry, Chinese J. Anal. Chem., 41, 1831–1836, doi:10.3724/sp.j.1096.2013.30545, 2013.

Liu, D., Allan, J., Whitehead, J., Young, D., Flynn, M., Coe, H., McFiggans, G., Fleming, Z. L., and Bandy, B.: Ambient black carbon particle hygroscopic properties controlled by mixing state and composition, Atmos. Chem. Phys., 13, 2015–2029, doi:10.5194/acp-13-2015-2013, 2013.

Liu, D., Allan, J. D., Young, D. E., Coe, H., Beddows, D., Fleming, Z. L., Flynn, M. J., Gallagher, M. W., Harrison, R. M., Lee, J., Prevot, A. S. H., Taylor, J. W., Yin, J., Williams, P. I., and Zotter, P.: Size distribution, mixing state and source apportionments of black carbon aerosols in London during winter time, Atmos. Chem. Phys. Discuss., 14, 16291–16349, doi:10.5194/acpd-14-16291-2014, 2014.

Size distribution and mixing state of BC particles in Shanghai

X. Gong et al.

Title Page

Abstract	Introduction
Conclusions	References
Tables	Figures

Back | Close

Full Screen / Esc

Printer-friendly Version

Interactive Discussion

Long, R. W., Eatough, N. L., Mangelson, N. F., Thompson, W., Fiet, K., Smith, S., Smith, R., Eatough, D. J., Pope, C. A., and Wilson, W. E.: The measurement of PM$_{2.5}$, including semi-volatile components, in the EMPACT program: results from the Salt Lake City Study, Atmos. Environ., 37, 4407–4417, doi:10.1016/S1352-2310(03)00585-5, 2003.

Matsui, H., Koike, M., Kondo, Y., Moteki, N., Fast, J. D., and Zaveri, R. A.: Development and validation of a black carbon mixing state resolved three-dimensional model: aging processes and radiative impact, J. Geophys. Res.-Atmos., 118, 2304–2326, doi:10.1029/2012JD018446, 2013.

McMeeking, G. R., Hamburger, T., Liu, D., Flynn, M., Morgan, W. T., Northway, M., Highwood, E. J., Krejci, R., Allan, J. D., Minikin, A., and Coe, H.: Black carbon measurements in the boundary layer over western and northern Europe, Atmos. Chem. Phys., 10, 9393–9414, doi:10.5194/acp-10-9393-2010, 2010.

Moffet, R. C. and Prather, K. A.: In-situ measurements of the mixing state and optical properties of soot with implications for radiative forcing estimates, P. Natl. Acad. Sci. USA, 106, 11872–11877, doi:10.1073/pnas.0900040106, 2009.

Moffet, R. C., de Foy, B., Molina, L. T., Molina, M. J., and Prather, K. A.: Measurement of ambient aerosols in northern Mexico City by single particle mass spectrometry, Atmos. Chem. Phys., 8, 4499–4516, doi:10.5194/acp-8-4499-2008, 2008.

Moteki, N., Kondo, Y., Miyazaki, Y., Takegawa, N., Komazaki, Y., Kurata, G., Shirai, T., Blake, D., Miyakawa, T., and Koike, M.: Evolution of mixing state of black carbon particles: aircraft measurements over the western Pacific in March 2004, Geophys. Res. Lett., 34, L11803, doi:10.1029/2006GL028943, 2007.

Moteki, N., Kondo, Y., and Nakamura, S.: Method to measure refractive indices of small nonspherical particles: application to black carbon particles, J. Aerosol Sci., 41, 513–521, doi:10.1016/j.jaerosci.2010.02.013, 2010.

Moteki, N., Kondo, Y., Oshima, N., Takegawa, N., Koike, M., Kita, K., Matsui, H., and Kajino, M.: Size dependence of wet removal of black carbon aerosols during transport from the boundary layer to the free troposphere, Geophys. Res. Lett., 39, L13802, doi:10.1029/2012GL052034, 2012.

Moteki, N., Kondo, Y., and Adachi, K.: Identification by single-particle soot photometer of black carbon particles attached to other particles: laboratory experiments and ground observations in Tokyo, J. Geophys. Res.-Atmos., 119, 1031–1043, doi:10.1002/2013JD020655, 2014.

Title Page

Abstract | Introduction

Conclusions | References

Tables | Figures

|◀ | ▶|

◀ | ▶

Back | Close

Full Screen / Esc

Printer-friendly Version

Interactive Discussion

Petzold, A., Ogren, J. A., Fiebig, M., Laj, P., Li, S.-M., Baltensperger, U., Holzer-Popp, T., Kinne, S., Pappalardo, G., Sugimoto, N., Wehrli, C., Wiedensohler, A., and Zhang, X.-Y.: Recommendations for reporting "black carbon" measurements, Atmos. Chem. Phys., 13, 8365–8379, doi:10.5194/acp-13-8365-2013, 2013.

Pöschl, U.: Atmospheric aerosols: composition, transformation, climate and health effects, Angew. Chem. Int. Edit., 44, 7520–7540, 2005.

Ramanathan, V. and Carmichael, G.: Global and regional climate changes due to black carbon, Nat. Geosci., 1, 221–227, 2008.

Reddington, C. L., McMeeking, G., Mann, G. W., Coe, H., Frontoso, M. G., Liu, D., Flynn, M., Spracklen, D. V., and Carslaw, K. S.: The mass and number size distributions of black carbon aerosol over Europe, Atmos. Chem. Phys., 13, 4917–4939, doi:10.5194/acp-13-4917-2013, 2013.

Riemer, N., Vogel, H., and Vogel, B.: Soot aging time scales in polluted regions during day and night, Atmos. Chem. Phys., 4, 1885–1893, doi:10.5194/acp-4-1885-2004, 2004.

Sahu, L. K., Kondo, Y., Moteki, N., Takegawa, N., Zhao, Y., Cubison, M. J., Jimenez, J. L., Vay, S., Diskin, G. S., Wisthaler, A., Mikoviny, T., Huey, L. G., Weinheimer, A. J., and Knapp, D. J.: Emission characteristics of black carbon in anthropogenic and biomass burning plumes over California during ARCTAS-CARB 2008, J. Geophys. Res.-Atmos., 117, D16302, doi:10.1029/2011jd017401, 2012.

Schnaiter, M., Linke, C., Mohler, O., Naumann, K. H., Saathoff, H., Wagner, R., Schurath, U., and Wehner, B.: Absorption amplification of black carbon internally mixed with secondary organic aerosol, J. Geophys. Res.-Atmos., 110, D19204, doi:10.1029/2005jd006046, 2005.

Schwarz, J. P., Gao, R. S., Fahey, D. W., Thomson, D. S., Watts, L. A., Wilson, J. C., Reeves, J. M., Darbeheshti, M., Baumgardner, D. G., Kok, G. L., Chung, S. H., Schulz, M., Hendricks, J., Lauer, A., Karcher, B., Slowik, J. G., Rosenlof, K. H., Thompson, T. L., Langford, A. O., Loewenstein, M., and Aikin, K. C.: Single-particle measurements of midlatitude black carbon and light-scattering aerosols from the boundary layer to the lower stratosphere, J. Geophys. Res.-Atmos., 111, D16207, doi:10.1029/2006jd007076, 2006.

Schwarz, J. P., Gao, R. S., Spackman, J. R., Watts, L. A., Thomson, D. S., Fahey, D. W., Ryerson, T. B., Peischl, J., Holloway, J. S., Trainer, M., Frost, G. J., Baynard, T., Lack, D. A., de Gouw, J. A., Warneke, C., and Del Negro, L. A.: Measurement of the mixing state, mass, and optical size of individual black carbon particles in urban and biomass burning emissions, Geophys. Res. Lett., 35, L13810, doi:10.1029/2008gl033968, 2008.

Title Page

Abstract | Introduction

Conclusions | References

Tables | Figures

|◄ | ►|

◄ | ►

Back | Close

Full Screen / Esc

Printer-friendly Version

Interactive Discussion

Schwarz, J. P., Spackman, J. R., Gao, R. S., Perring, A. E., Cross, E., Onasch, T. B., Ahern, A., Wrobel, W., Davidovits, P., Olfert, J., Dubey, M. K., Mazzoleni, C., and Fahey, D. W.: The detection efficiency of the single particle soot photometer, Aerosol Sci. Tech., 44, 612–628, doi:10.1080/02786826.2010.481298, 2010.

Seinfeld, J. H. and Pandis, S. N.: Atmospheric chemistry and physics: from air pollution to climate change, John Wiley & Sons, Hoboken, New Jersey, 2006.

Shiraiwa, M., Kondo, Y., Iwamoto, T., and Kita, K.: Amplification of light absorption of black carbon by organic coating, Aerosol Sci. Tech., 44, 46–54, doi:10.1080/02786820903357686, 2010.

Sodeman, D. A., Toner, S. M., and Prather, K. A.: Determination of single particle mass spectral signatures from light-duty vehicle emissions, Environ. Sci. Technol., 39, 4569–4580, doi:10.1021/es0489947, 2005.

Song, X. H., Hopke, P. K., Fergenson, D. P., and Prather, K. A.: Classification of single particles analyzed by ATOFMS using an artificial neural network, ART-2A, Anal. Chem., 71, 860–865, doi:10.1021/ac9809682, 1999.

Soto-García, L. L., Andreae, M. O., Andreae, T. W., Artaxo, P., Maenhaut, W., Kirchstetter, T., Novakov, T., Chow, J. C., and Mayol-Bracero, O. L.: Evaluation of the carbon content of aerosols from the burning of biomass in the Brazilian Amazon using thermal, optical and thermal-optical analysis methods, Atmos. Chem. Phys., 11, 4425–4444, doi:10.5194/acp-11-4425-2011, 2011.

Stephens, M., Turner, N., and Sandberg, J.: Particle identification by laser-induced incandescence in a solid-state laser cavity, Appl. Optics, 42, 3726–3736, doi:10.1364/ao.42.003726, 2003.

Takahama, S., Russell, L. M., Shores, C. A., Marr, L. C., Zheng, J., Levy, M., Zhang, R., Castillo, E., Rodriguez-Ventura, J. G., Quintana, P. J. E., Subramanian, R., Zavala, M., and Molina, L. T.: Diesel vehicle and urban burning contributions to black carbon concentrations and size distributions in Tijuana, Mexico, during the Cal-Mex 2010 campaign, Atmos. Environ., 88, 341–352, doi:10.1016/j.atmosenv.2013.09.057, 2014.

Taylor, J. W., Allan, J. D., Liu, D., Flynn, M., Weber, R., Zhang, X., Lefer, B. L., Grossberg, N., Flynn, J., and Coe, H.: Assessment of the sensitivity of core/shell parameters derived using the single-particle soot photometer to density and refractive index, Atmos. Meas. Tech. Discuss., 7, 5491–5532, doi:10.5194/amtd-7-5491-2014, 2014.

Size distribution and mixing state of BC particles in Shanghai

X. Gong et al.

Title Page

Abstract | Introduction

Conclusions | References

Tables | Figures

|◄ | ►|

◄ | ►

Back | Close

Full Screen / Esc

Printer-friendly Version

Interactive Discussion

Toner, S. M., Sodeman, D. A., and Prather, K. A.: Single particle characterization of ultrafine and accumulation mode particles from heavy duty diesel vehicles using aerosol time-of-flight mass spectrometry, Environ. Sci. Technol., 40, 3912–3921, doi:10.1021/es051455x, 2006.

Wang, X., Ye, X., Chen, H., Chen, J., Yang, X., and Gross, D. S.: Online hygroscopicity and chemical measurement of urban aerosol in Shanghai, China, Atmos. Environ., 95, 318–326, doi:10.1016/j.atmosenv.2014.06.051, 2014.

Ye, B., Ji, X., Yang, H., Yao, X., Chan, C. K., Cadle, S. H., Chan, T., and Mulawa, P. A.: Concentration and chemical composition of $PM_{2.5}$ in Shanghai for a 1 year period, Atmos. Environ., 37, 499–510, doi:10.1016/S1352-2310(02)00918-4, 2003.

Zhang, G., Bi, X., He, J., Chen, D., Chan, L. Y., Xie, G., Wang, X., Sheng, G., Fu, J., and Zhou, Z.: Variation of secondary coatings associated with elemental carbon by single particle analysis, Atmos. Environ., 92, 162–170, doi:10.1016/j.atmosenv.2014.04.018, 2014.

Zhang, R., Khalizov, A. F., Pagels, J., Zhang, D., Xue, H., and McMurry, P. H.: Variability in morphology, hygroscopicity, and optical properties of soot aerosols during atmospheric processing, P. Natl. Acad. Sci. USA, 105, 10291–10296, doi:10.1073/pnas.0804860105, 2008.

Size distribution and mixing state of BC particles in Shanghai

X. Gong et al.

Title Page

Abstract	Introduction
Conclusions	References
Tables	Figures

|◄   ►|

◄   ►

Back   Close

Full Screen / Esc

Printer-friendly Version

Interactive Discussion

Table 1. Names, numbers and fractions of seven types of BC-containing particles detected by the SPAMS instrument.

Group	Number of particles	Fraction of particles
Pure BC	452	0.53 %
Biomass Burning BC-containing (BBBC)	19 446	22.60 %
K-rich BC-containing (KBC)	8782	10.20 %
NaK-rich BC-containing (NaKBC)	5819	6.76 %
BC internally-mixed with OC and ammonium nitrate (BCOC-NOx)	33 336	38.74 %
BC internally-mixed with OC and ammonium sulfate (BCOC-SOx)	15 101	17.55 %
Unidentified	3121	3.63 %
Total BC-containing	86 057	100 %
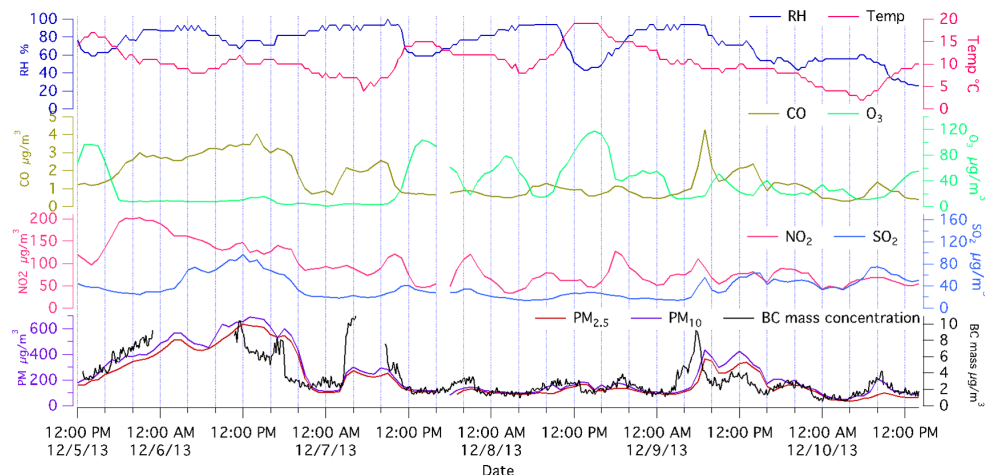
Figure 1. Temporal profiles of selected meteorological parameters (temperature, relative humidity) with 30 min resolution, gaseous pollutants (CO, O_3, SO_2 and NO_2), $PM_{2.5}$ and PM_{10} mass concentrations with 60 min resolution were provided by Shanghai Environmental Monitoring Center, Hongkou Station (http://www.semc.com.cn/aqi/home/Index.aspx). The station is 3.3 km away from the sampling site. The concentration of BC mass (10 min resolution) was continuously measured by SP2 at the sampling site.

Title Page

Abstract · Introduction

Conclusions · References

Tables · Figures

Back · Close

Full Screen / Esc

Printer-friendly Version

Interactive Discussion
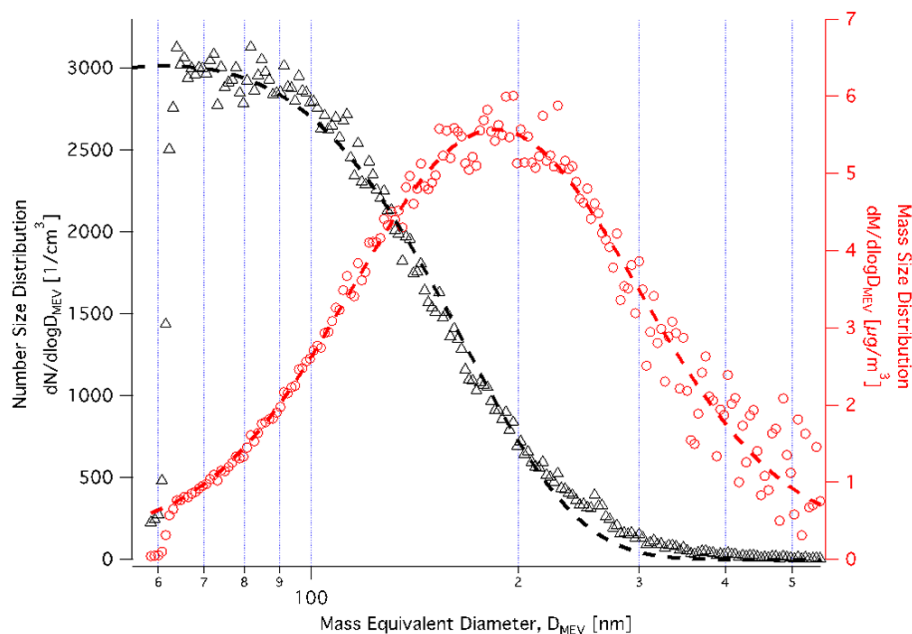
Figure 2. The measured BC core mass size distribution and number size distribution are shown in open red and black markers, respectively. The log-normal fitting to the observed distributions are shown by the dashed lines.

Discussion Paper | Discussion Paper | Discussion Paper | Discussion Paper |

ACPD

15, 35383–35415, 2015

Size distribution and mixing state of BC particles in Shanghai

X. Gong et al.

Title Page

Abstract | Introduction

Conclusions | References

Tables | Figures

|◀ | ▶|

◀ | ▶

Back | Close

Full Screen / Esc

Printer-friendly Version

Interactive Discussion
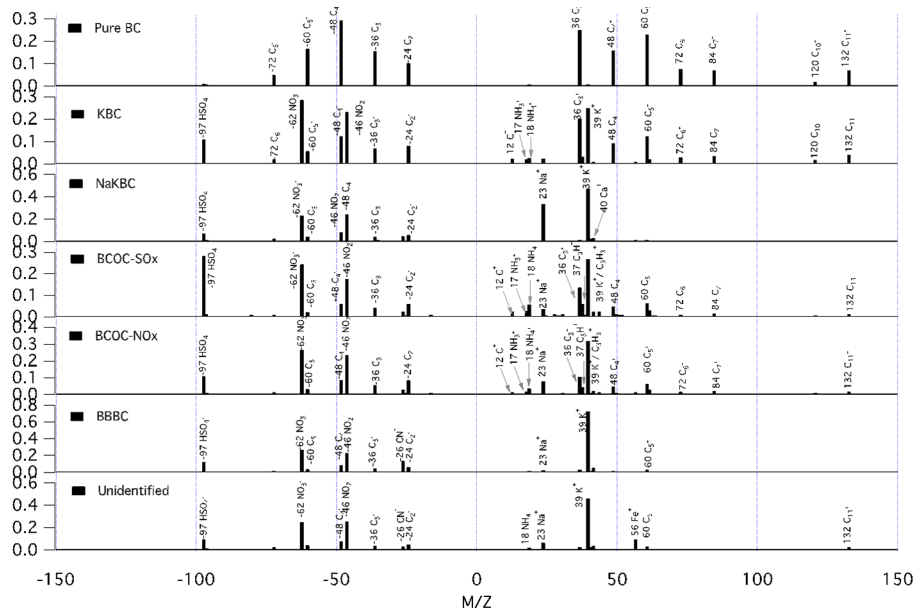
Figure 3. Averaged mass spectra of different types of BC-containing particles. Major peaks are labeled with the most probable assignments.
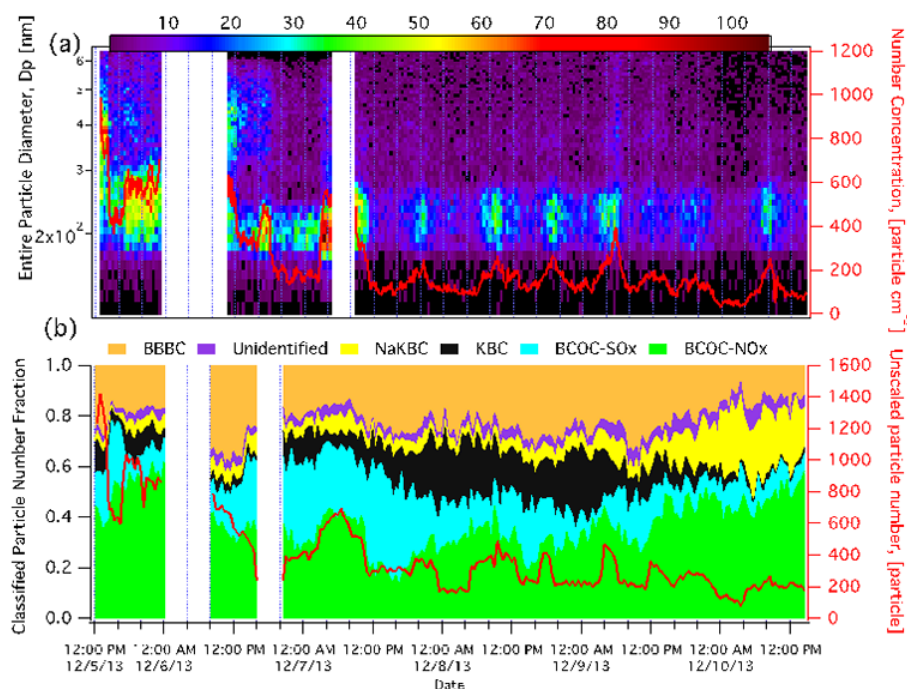
Figure 4. (a) Temporal variations of BC-containing particles number and size distributions with 30 min resolution. The red line shows the number concentration of total BC-containing particles (detected by SP2). **(b)** Temporal variation of number fractions of different BC-containing particle types with 10 min time resolution. The red line shows the number concentration of total BC-containing particles (detected by SPAMS).
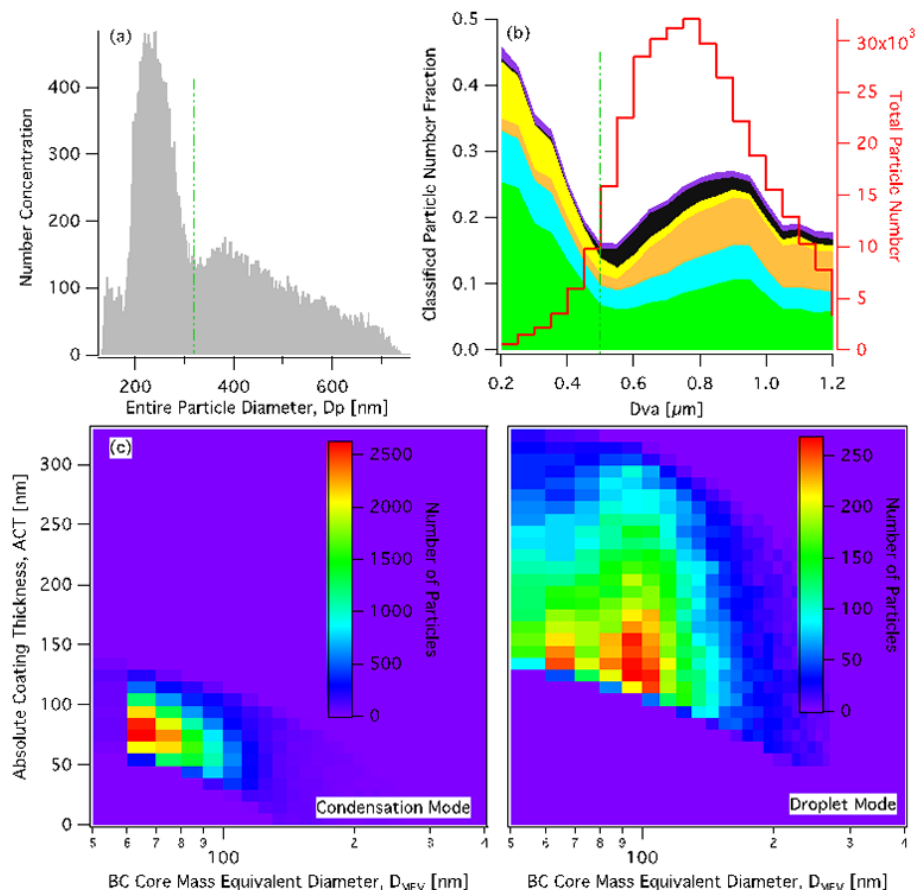
Figure 5. (a) D_p number size distribution histogram for the SP2-detected BC-containing particles. **(b)** D_{va} number fraction distribution of SPAMS-detected different types BC-containing particles. **(c)** D_c and ACT with number size distribution in the condensation and droplet modes.
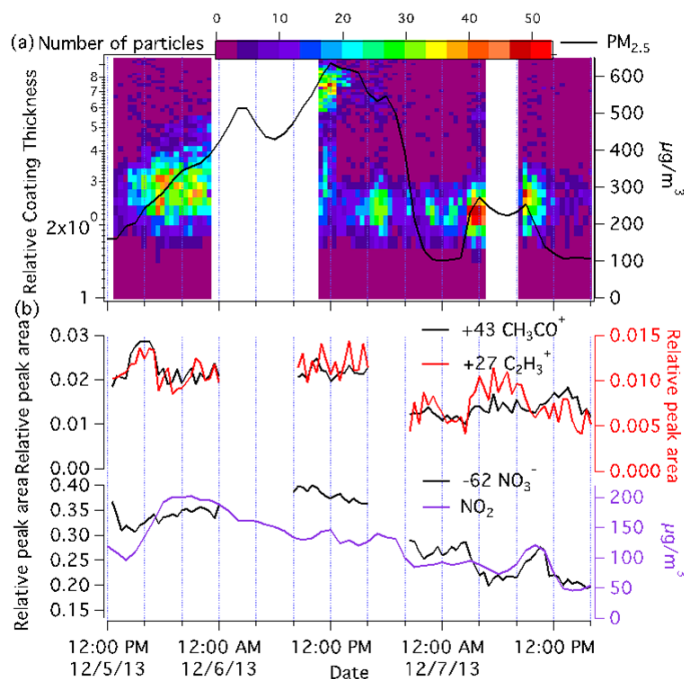
Figure 6. (a) Temporal variation of the relative coating thickness distribution of traffic-emitted BC-containing particles (SP2) with 30 min resolution and the temporal profile of $PM_{2.5}$ concentration with 60 min resolution. **(b)** Temporal variation of relative peak areas of $^{27}C_2H_3^+$, $^{43}CH_3CO^+$, $^{62}NO_3^-$ of traffic-emitted BC-containing particles (SPAMS) and NO_2 concentration with 30 min resolution.

Size distribution and mixing state of BC particles in Shanghai

X. Gong et al.

Title Page

Abstract	Introduction
Conclusions	References
Tables	Figures

|◄   ►|

◄   ►

Back   Close

Full Screen / Esc

Printer-friendly Version

Interactive Discussion